The Journal of Experimental Biology 215, 3231-3241

doi:10.1242/jeb.068981

RESEARCH ARTICLE

Rajiform locomotion: three-dimensional kinematics of the pectoral fin surface during swimming in the freshwater stingray *Potamotrygon orbignyi*

Erin L. Blevins* and George V. Lauder

Museum of Comparative Zoology, Harvard University, 26 Oxford Street, Cambridge, MA 02138, USA

*Author for correspondence (eblevins@fas.harvard.edu)

SUMMARY

Rajiform locomotion in fishes is dominated by distinctive undulations of expanded pectoral fins. Unlike other fishes, which typically interact with the fluid environment *via* multiple fins, undulating rays modulate a single control surface, the pectoral disc, to perform pelagic locomotion, maneuvering and other behaviors. Complex deformations of the broad, flexible pectoral fins occur as the undulating wave varies in three dimensions; pectoral fin kinematics and changes in waveform with swimming speed cannot be fully quantified by two-dimensional analyses of the fin margin. We present the first three-dimensional analysis of undulatory rajiform locomotion in a batoid, the freshwater stingray *Potamotrygon orbignyi*. Using three cameras (250 frames s^{-1}), we gathered three-dimensional excursion data from 31 points on the pectoral fin during swimming at 1.5 and 2.5 disc lengths s^{-1}, describing the propulsive wave and contrasting waveforms between swimming speeds. Only a relatively small region of the pectoral fin (~25%) undulates with significant amplitude (>0.5 cm). Stingrays can maintain extreme lateral curvature of the distal fin margin in opposition to induced hydrodynamic loads, 'cupping' the edge of the pectoral fin into the flow, with potential implications for drag reduction. Wave amplitude increases across both anteroposterior and mediolateral fin axes. Along the anteroposterior axis, amplitude increases until the wave reaches mid-disc and then remains constant, in contrast to angulliform patterns of continuous amplitude increase. Increases in swimming speed are driven by both wave frequency and wavespeed, though multivariate analyses reveal a secondary role for amplitude.

Supplementary material available online at http://jeb.biologists.org/cgi/content/full/215/18/3231/DC1

Key words: batoid, ray, elasmobranch, fish, undulation.

Received 2 December 2011; Accepted 1 June 2012

INTRODUCTION

Fish interact with the fluid environment using a variety of surfaces – paired fins, median fins and the body itself (Harris, 1936; Standen and Lauder, 2005; Standen and Lauder, 2007; Tytell et al., 2008; Webb, 2006). These multiple control surfaces work in combination to produce thrust and balance torques in steady swimming, to maneuver and, at evolutionary time scales, may offer redundant systems, allowing one set of fins to specialize for a particular function while others drive locomotion (e.g. pelvic 'sucker discs' in Liparidae, dorsal fin 'fishing lures' in Lophiidae). In contrast, rays (Batoidea) perform virtually all behaviors using a single broad surface: the distinctive, expanded pectoral fins. Pelvic fins are also employed by benthic skates and rays as they move along the substrate (Macesic and Kajiura, 2010), but the pectoral fins also control functions that range from epibenthic and pelagic locomotion to prey capture and camouflage, as rays bury themselves or search for food in the substrate (Wilga et al., 2012).

Locomotion by rays and skates has been set apart since early classifications of swimming modes, with the eponymous 'rajiform mode' originally encompassing locomotion by any elasmobranch with expanded pectoral fins, from manta rays (Myliobatidae: Mobulinae) to stingrays (Dasyatidae) (Breder, 1926). Most batoids do use their pectoral fins to swim, with the exception of body-caudal fin propulsion by guitarfish (Rhiniformes and Rhynchobatiformes; Klausewitz, 1965) and torpedo rays (Torpediniformes; Roberts, 1969). However, even among pectoral-fin swimmers, fin morphology and kinematics vary widely. More recent work has recognized the diversity of locomotion within the group, distinguishing two modes: (1) mobuliform oscillation, underwater flapping flight dominated by dorsoventral excursion, and (2) rajiform undulation, *via* a propulsive wave of bending that passes from anterior to posterior along the pectoral fin (Webb, 1994). Rosenberger (Rosenberger, 2001) identified a continuum of batoid locomotion between oscillation and undulation, with species' position between the two extremes defined by the number of waves present on the pectoral fin at one time; undulators have more than one wave, oscillators less than one. The distinction is more than kinematic: oscillators are typically pelagic, and have high-aspect-ratio fins, whereas undulators are primarily benthic, with a low-aspect-ratio pectoral disc (Rosenberger, 2001). Skeletal morphology also reflects locomotor mode, with areas of increased fin stiffness and preferential axes of bending created by the arrangement of fin-radial joints and variations in calcification pattern (Schaefer and Summers, 2005).

Both oscillatory and undulatory rays are popular inspirations for biomimetic designs. Studies of mobuliform locomotion have found surprising maneuverability and efficiency in manta rays and other, typically large, 'underwater fliers' (Heine, 1992; Parson et al., 2011); the charismatic manta is the basis of several bio-inspired robots (e.g. Moored et al., 2011). Mathematical models suggest interesting fluid properties for undulating rays as well; vortices may be retained in the troughs of an undulating fin, acting as 'fluid roller bearings'

that reduce drag (Wu et al., 2007), whereas stingray-like 'waving plates' may relaminarize flow (Taneda and Tomonari, 1974). Opportunities to investigate these phenomena are increasing as advances in robotics and new, flexible biomaterials make undulatory locomotion a practical model for biomimesis. Models of knifefish (Curet et al., 2011), undulatory rays and ray-like fins (Low, 2006; Clark and Smits, 2006) may be based on different organisms, but they share the same underlying principle: locomotion is controlled by a single undulating surface, with modulations of the wave function producing steady swimming, acceleration or more complex maneuvers.

The fins of undulating rays and their robotic counterparts are both broad and highly flexible, as they must have sufficient area to generate thrust and the capacity to bend into various waveforms. This combination of flexibility and breadth creates a large parameter space of possible waves; waveforms are truly three-dimensional (3-D), and may vary along both anteroposterior and mediolateral axes (i.e. both fin chord and span). Changes in waveform may occur *via* the direct action of dorsal and ventral fin muscles during wave propagation, as seen in the blue-spot stingray, *Taenuria lymma* (Rosenberger and Westneat, 1999). They could also result from variations in overall fin structure (Schaefer and Summers, 2005) or the shape and stiffness of individual fin elements, as Taft et al. (Taft et al., 2008) found to influence pectoral fin motion in sculpin.

In this study, we analyze pectoral fin undulation in three dimensions, determining the kinematics of the propulsive wave in steady swimming by the freshwater stingray *Potamotrygon orbignyi*, an undulatory swimmer. Previous work on undulating rays has described the propulsive wave in terms of the motion of a single point at the fin margin (Rosenberger, 2001), or several points along the margin (Rosenberger and Westneat, 1999), but has not explored the pectoral fin as an undulating surface. Here, we ask how the propulsive wave changes as it propagates across the pectoral fin, and determine what modulations occur with increased swimming speed. In most fishes, increases in the frequency of propulsive motions drive increases in swimming speed (e.g. increased tailbeat frequency) while amplitude remains constant (Bainbridge, 1958; Drucker and Jensen, 1996). However, in the only detailed study of stingray swimming kinematics, Rosenberger and Westneat (Rosenberger and Westneat, 1999) found that the swimming speed of *T. lymma* was frequency-modulated in some cases, and amplitude-modulated in others, depending on the individual. We therefore expect similar individual variation in *P. orbignyi*, with swimming speed driven by either the frequency or amplitude of the pectoral wave. Within speeds, we predict that amplitude will increase along both anteroposterior and mediolateral axes, and that the wave will accelerate as it propagates. To test our hypotheses and describe the 3-D wave, we gathered detailed 3-D excursion data from 31 points across the pectoral fin surface, determining wave properties and values for fin curvature. We compare and contrast waveforms between the two swimming speeds, discovering how pectoral undulations are modulated to increase velocity.

MATERIALS AND METHODS

Animals

Juvenile freshwater stingrays, *Potamotrygon orbignyi* (Castelnau 1855), were purchased from a local importer and transported to Harvard University (Cambridge, MA, USA). We chose to work with juvenile potamotrygonids because their small size [mean pectoral disc length (DL) 12.8±0.8 cm, mean disc width (DW) 11.27±0.99 cm] allowed the study of undulatory swimming in a small, controlled volume, yielding high-resolution kinematic data. In the laboratory, stingrays were housed in individual 100 liter aquaria with >2 cm of sandy substrate (grain size 1–3 mm). Animals were maintained at 27±1°C under a 12 h:12 h light:dark photoperiod, and were fed live blackworms six times per week. Three individuals were used in our experiments, with all animal care performed according to Harvard University IACUC protocols (no. 20-03).

Swimming protocol and videography

Stingrays were filmed while swimming in a calibrated, variable-speed flow tank (see Tytell and Lauder, 2004), heated to 27±1°C, at a Reynolds number of approximately 10,000. Baffles constructed of plastic mesh (0.5 cm mesh size) were positioned upstream and downstream to restrict stingrays to the working section (28×28×66 cm, width × height × length). A third, angled baffle was placed ventral to the stingray to encourage swimming, preventing stingrays from settling to the flat flow-tank bottom where they could remain motionless even in high flow. The baffle was positioned with its upstream end higher than its downstream end, forming an angle of ~20 deg with the tank bottom. We verified that fluid maintained micro-turbulent flow and steady velocity as it passed through the angled baffle, and analyzed only swimming sequences where stingrays swam well clear of all baffles and flow tank surfaces. We used a wooden dowel to maneuver animals away from the sides of the flow tank, but removed it before filming. Individual stingrays were filmed during steady swimming at two speeds, 1.5 and 2.5 DL s^{-1} (approximately 0.20 and 0.33 m s^{-1}, respectively).

Swimming sequences were recorded at 250 frames s^{-1} by three synchronized, one-megapixel high-speed video cameras (FASTCAM 1024 PCI; Photron USA, San Diego, CA, USA). One camera captured a dorsal view *via* a 45 deg angled mirror positioned above the flow tank, and the remaining two cameras were set off-axis from dorsal and lateral positions. Camera height and angles ensured that all portions of the stingray pectoral fin were visible in at least two camera views throughout each finbeat. (One finbeat was defined as a full cycle of the propulsive wave.) As cameras were widely spaced to film stingrays from different angles, this allowed kinematics to be reconstructed in 3-D. Cameras were calibrated using direct linear transformation (DLT) to remove image distortion and align camera views in 3-D space, using the DLT Calibration 3 program in MATLAB version 7.10 (MathWorks, Natick, MA, USA) (Hedrick, 2008).

Kinematic measurements and analysis

To determine the 3-D kinematics of undulation and variations with swimming speed, we analyzed four finbeats from each of three individuals for two speeds, for a total of 24 sequences. Finbeats were defined as a full cycle of the propulsive wave, from the initiation of a wave at the anterior edge of the fin through completion as the wave passed off the posterior edge. Using the DLT Dataviewer 2 program in MATLAB version 7.10 (Hedrick, 2008), we digitized 31 points across the right pectoral fin and along the body midline, determining the x, y and z coordinates of each point in every frame *via* direct linear transformation to give fin surface deformations in 3-D (Fig. 1). Natural pigmentation markings on the dorsal surface of the pectoral fin allowed the same points to be reliably identified in each camera view. After initial analysis confirmed that the body midline does not undulate, we slightly reduced the number of midline points analyzed, and present results based on 29 digitized points.

Throughout the paper, we present standardized measurements relative to disc length, disc width and disc perimeter (DP) (*sensu* Rosenberger and Westneat, 1999; Rosenberger, 2001). Disc length

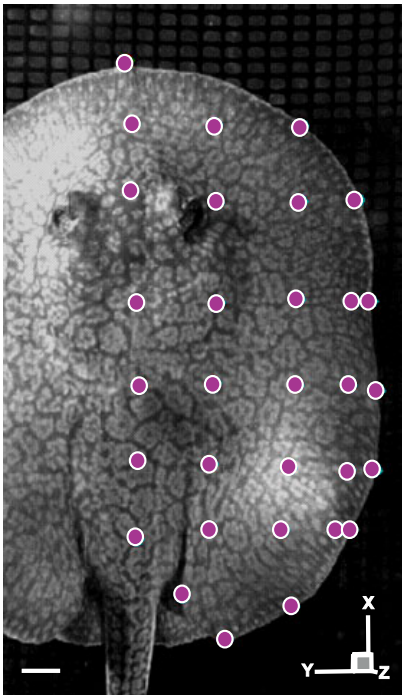

Fig. 1. Dorsal view of freshwater stingray *Potamotrygon orbignyi* (anterior at top); purple circles indicate the locations of the 31 points digitized on the dorsal surface of the right pectoral fin. Scale bar, 1 cm.

was measured from the most anterior point on the stingray snout to the posterior margin of the pectoral fin disc, and is equivalent to chord length. Disc width was determined as the distance from the lateral edge of one pectoral fin to the other, at the widest part of the pectoral fin disc, and is equivalent to fin span. For each swimming sequence, mean values were determined for kinematic variables including the amplitude, frequency, wavespeed and wavelength of the propulsive wave, plus the whole-body angle of attack and spanwise fin curvature. These variables (frequency, amplitude, wavespeed and wavelength) allow us to characterize the pectoral fin wave as it propagates across the surface of the fin, and determine additional features of stingray locomotion (angle of attack, fin curvature) that influence the interactions of fish and fluid. We compare these variables between speeds to quantify the kinematic changes that increase thrust and allow stingrays to swim faster. Amplitude was calculated for each point as half of the total dorsoventral excursion. We determined amplitude variation along the fin, and also compared total amplitude (the sum of average amplitudes for all points) between swimming speeds, as a metric to represent the volume through which the fin travels during one wave cycle. For comparison with 2-D kinematic data from previous work (e.g. Rosenberger, 2001), we determined a mid-disc value for amplitude at 0.5 DL, corresponding to maximum disc width. Frequency (f) was determined as the number of wave cycles per second at mid-disc. To determine wavespeed (v), we chose a known distance between points along an anteroposterior axis, and then divided that distance by the time required for a given wave (e.g. crest or trough) to travel that distance. We calculated a mid-disc wavespeed at 0.5 DL along the distal margin of the fin and, to examine variation across the fin surface, determined local wavespeeds at points along three anteroposterior transects spaced at different distances from the midline. Wavespeed and frequency are not reported for every point individually, as variations are subtle and require a pronounced (high amplitude) wave for reliable calculation. Wavelength (λ) was determined by dividing mid-disc wavespeed (v) by mid-disc frequency (f), according to the wave function $\lambda=v/f$. We calculated slip and stride length as two common measures of propulsive efficiency, which relate the motion of the pectoral fin to the overall forward progress of the stingray body (see Rosenberger, 2001). Slip was calculated as the ratio of overall swimming speed (U) to the velocity of the propulsive wave (v); stride length was defined as the distance traveled per wave cycle, the ratio of forward swimming speed (U) to propulsive wave frequency (f). Strouhal number was determined by fL/U, with disc length used as the characteristic length L. Wave number, defined as the number of waves present on the fin at one time, was calculated relative to both disc length and disc perimeter. To determine body angle of attack, the angle between the body and oncoming water flow, we performed a linear regression of at least five digitized points along the stingray midline, and then determined the angle between the regression line and the horizontal axis (x-axis, parallel to the direction of flow) in each video frame. Fin curvature (κ) was determined at each time step for three-point mediolateral transects in the mid-disc region (middle third of the fin), at the distal margin of the fin. We calculated curvature using standard methods (see Standen and Lauder, 2005; Taft et al., 2008), *via* the following equation:

$$\kappa = |d\mathbf{T}/ds| \, , \quad (1)$$

where s is the arc length of a curve connecting all three points in the transect and $\mathbf{T}$ is the unit tangent vector of that curve. We determined values for maximum positive (concave up) and negative (concave down) curvature. The percentage of a wave cycle spent in negative curvature was determined by dividing the time spent in negative curvature by total cycle time. Beyond the results presented here, we offer detailed kinematic data sets as supplementary material (Tables S1, S2, Fig. S1).

Statistical analysis

A mixed-model two-factor ANOVA was performed in JMP 9.0.2 (SAS Institute, Cary, NC, USA) to test the effects of swimming speed and individual on all kinematic variables. To compare local wavespeeds determined at different points across the fin surface, and test for differences in wavespeed based on position, we used a second ANOVA and a *post hoc* Tukey's test. To examine multivariate differences between swimming speeds, we performed a principal component analysis (PCA) on 11 variables: mid-disc amplitude, frequency, wavespeed, wavelength, body angle, maximum amplitude, location of maximum amplitude, maximum negative curvature, maximum positive curvature, portion of cycle spent in negative curvature, and total excursion. A multivariate ANOVA (MANOVA) was performed to test for group separation along PCA axes. All variables except the location of maximum amplitude were major elements of the first four principal components, and were retained in a discriminant function analysis (DFA). Analyses were performed in JMP 9.0.2; values are given as means ± s.e.m.

RESULTS

Pectoral wave and body kinematics

Pectoral fin locomotion in *P. orbignyi* occurs *via* a propulsive wave passing from anterior to posterior along the fin (Figs 2, 3). At mid-disc (maximum disc width), the wave has a mean amplitude of 1.41±0.06 cm, increasing to a maximum amplitude of 1.66±0.04 cm

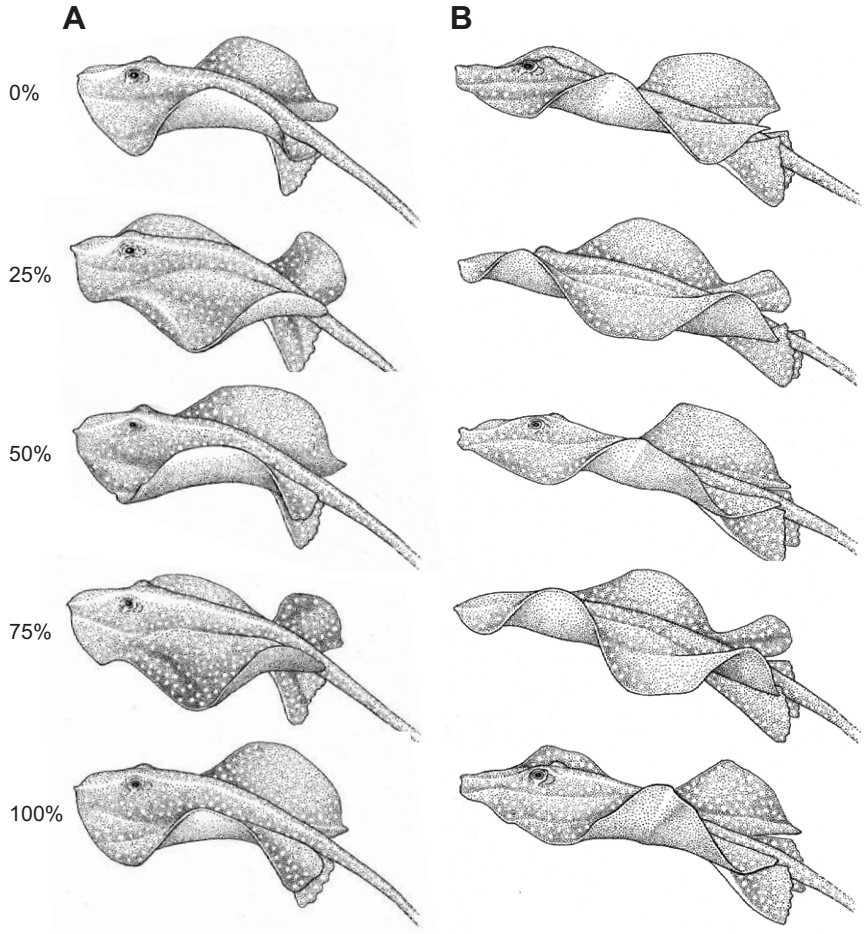

Fig. 2. Illustration of *P. orbignyi* swimming at (A) 1.5 disc lengths (DL) s^{-1} and (B) 2.5 DL s^{-1}, at intervals of 25% of one finbeat. Stingrays are shown in a three-quarter lateral view, angled slightly toward the dorsal and posterior to best show the propulsive wave. In the first row of images, a propulsive wave is initiated at the anterior edge of the pectoral fin (0% of the finbeat). As the cycle progresses, the wave passes along the pectoral fin, increasing in amplitude (25–75% of the finbeat), then passing off the posterior margin of the disc (100% of the finbeat). Note differences in wave timing between swimming speeds. However, overall findings for body angle are not reflected by the particular sample images and view angles used here.

approximately 2 cm posterior to the mid-disc; neither mid-disc nor maximum amplitude changes significantly with speed (ANOVA, P=0.74 and 0.88, respectively; Fig. 4A). The location of maximum amplitude also remains constant across speeds, occurring at ~0.7 DL (ANOVA, P=0.90). Frequency, mid-disc wavespeed and body angle all increase significantly with swimming speed (Fig. 4B–D). Frequency increases from 2.53±0.16 to 3.80±0.18 Hz (ANOVA, P<0.0001) and mid-disc wavespeed from 31.00±2.53 to 46.02±3.25 cm s^{-1} (ANOVA, P<0.01), a 50% increase in each value with a 65% increase in swimming speed. We calculated a mean wavelength of 12.5±0.7 cm, which did not vary across speeds (ANOVA, P=0.89); standardized to disc length and disc perimeter, this equates to a wave number of 1.10±0.08 (DL) or 1.65±0.12 (DP). Body angle increases as stingrays swim faster, from 5.1±1.1 to 7.8±0.7 deg (ANOVA, P<0.05), though this finding is not illustrated by the particular sample images and view angles depicted in Fig. 2. Stingrays swam with a slip of 0.7±0.04 and a stride length of 8.7±0.3 cm, at Strouhal number 0.2±0.01; none of these values differed significantly with swimming speed (ANOVA, P>0.2).

Kinematic variation across the fin surface

We examined variation in amplitude and wavespeed across the fin surface. Amplitude increases along both anteroposterior and mediolateral axes, with the highest excursion occurring in the distal posterior region of the fin (Fig. 2, Fig. 5A). Total amplitude, the sum of pectoral fin amplitude at all positions, is 16.82±0.62 cm, and does not vary with swimming speed (Fig. 5B; ANOVA, P=0.48). The mediolateral trend reflects increasing angular displacement with distance from the midline (Fig. 6). Along the anteroposterior axis, amplitude is negligible from the anterior margin until ~0.3 DL (i.e. values within the margin of experimental measurements, as demonstrated by the amplitude measured at non-oscillating midline points) (Fig. 7). Amplitude increases between 0.3 and ~0.5 DL; the rate of increase slows as the wave moves towards the posterior region of the fin, approaching an asymptote. The magnitude of the asymptote depends on the distance from the midline, with points further from the midline having a higher asymptote (and greater maximum amplitude) because of increasing angular displacement along the fin's span. For all points except one, amplitudes remain constant across swimming speeds (ANOVA, P>0.05); the exceptional point is located just distal to the tail, where the pectoral fin forms a lobe at its posterior margin, with an amplitude inversely correlated to swimming speed, decreasing from 0.88±0.07 to 0.58±0.05 cm (ANOVA, P<0.01). In addition to the data discussed here, supplementary materials provide mean excursion data for all points (supplementary material Table S1, Fig. S1) and a sample data set (x, y and z coordinates) for one wave cycle (supplementary material Table S2, with animation shown in supplementary material Movie 1).

Local wavespeeds determined at points from 0.4 to 0.7 DL generally reflect the mid-disc value and do not vary significantly with swimming speed (Fig. 8). Distal wavespeeds show no variation along the anteroposterior axis (ANOVA, P>0.05). Medially, however, wavespeeds do vary along the length of the disc (ANOVA, P=0.0001); a *post hoc* Tukey's test identified the medial, posterior wavespeed as significantly different from medial-anterior and medial-intermediate wavespeeds. At both swimming speeds, medial wavespeeds show a similar pattern, decreasing (though not

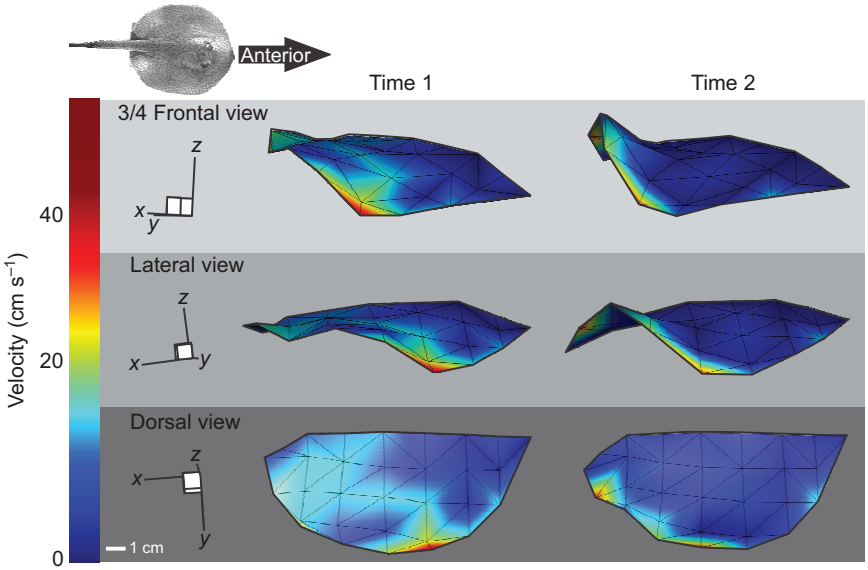

Fig. 3. Sample images showing pectoral fin motion in three dimensions, in three-quarter frontal, lateral and dorsal views, at two points in the wave cycle. To best portray the propulsive wave of the right pectoral fin, non-orthogonal perspectives are shown, and anterior is to the right. Images are reconstructed from digitized data points connected into a triangular mesh to model the fin surface. Colors indicate velocity magnitudes relative to the motion of the head, with greater magnitudes represented by warmer colors.

significantly) from anterior to intermediate positions, and then increasing posteriorly.

Mediolateral fin curvature

In addition to the anteroposterior bending that accompanies the propulsive wave, stingray fins show mediolateral curvature, with a maximum of 0.06±0.02 mm^{-1} in both positive (concave up) and negative (concave down) directions (Fig. 9A). No significant differences in the magnitude of curvature exist between swimming speeds, curvature direction (positive or negative) or along an anteroposterior axis from 0.4 to 0.7 DL (ANOVAs, P>0.1 for all comparisons). High-speed video stills from some sequences reveal extreme negative curvature of the distal fin, with a smaller radius than could be resolved given the limited number of points digitized in this region (Fig. 9B). The proportion of a wave cycle spent in negative curvature is highly variable. Although the mean value of 59±4% suggests a relatively even division of cycle time between positive and negative curvature, values range widely from 30 to 93%, and in almost one-third of sequences the fin is negatively curved for more than 75% of the cycle. There is no clear relationship between fin curvature and wave phase, and curvature can clearly persist across phases (Fig. 9B). However, two major patterns of curvature emerge. As the fin moves through a wave cycle, it may bend in the opposite direction to fin motion: concave down during the 'upstroke', as the wave moves from trough to crest, and concave up during the crest-to-trough 'downstroke' (Fig. 10A,B). Alternatively, the fin may retain concave-down curvature on both upstroke and downstroke (Fig. 10A,C). Concave-up curvature does not persist for any major portion of the upstroke.

Multivariate kinematic changes with swimming speed

A single principal component showed significant separation of groups by swimming speed (MANOVA, P<0.05), explaining 16.8% of sequence variation (Fig. 11A). Mid-disc wavespeed, mid-disc frequency and the proportion of the cycle spent in negative curvature loaded high on this axis. Groups were successfully separated by speed along the first canonical axis of the DFA (100% correct classifications), based on mid-disc wavespeed and mid-disc frequency, and (to a lesser degree) mid-disc amplitude, body angle and wavelength (Fig. 11B).

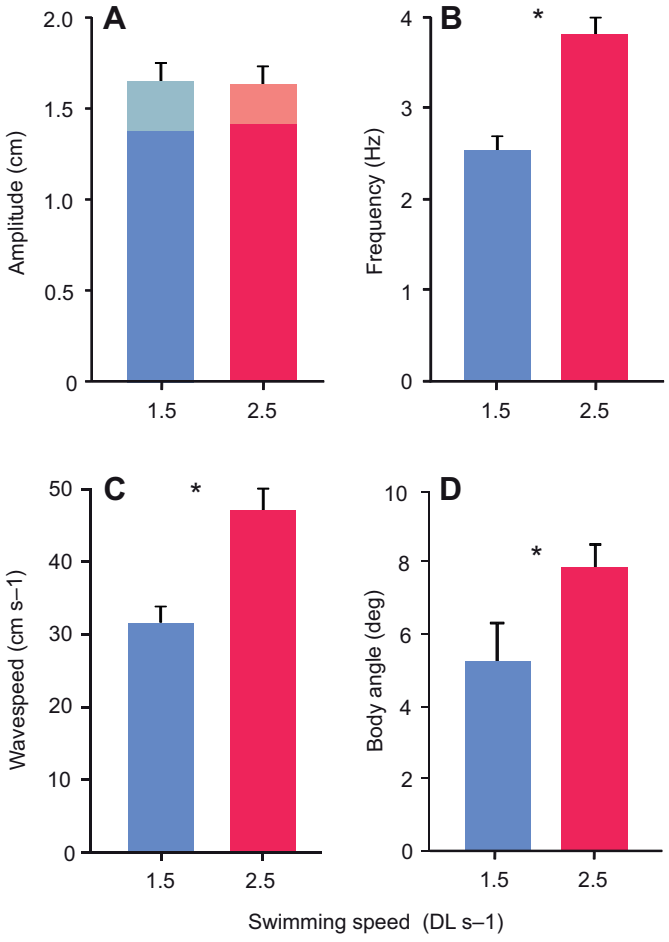

Fig. 4. Mean values of major kinematic variables at each swimming speed, 1.5 DL s^{-1} (blue) and 2.5 DL s^{-1} (red). (A) Amplitude, as mid-disc value (deep blue/red) and maximum amplitude (light blue/red); (B) frequency; (C) mid-disc wavespeed; (D) body angle, the incline of the dorsal midline relative to the horizontal. Asterisks indicate significant differences between swimming speeds (P<0.05); error bars represent 1 s.e.m. N=12 for all variables at each swimming speed.

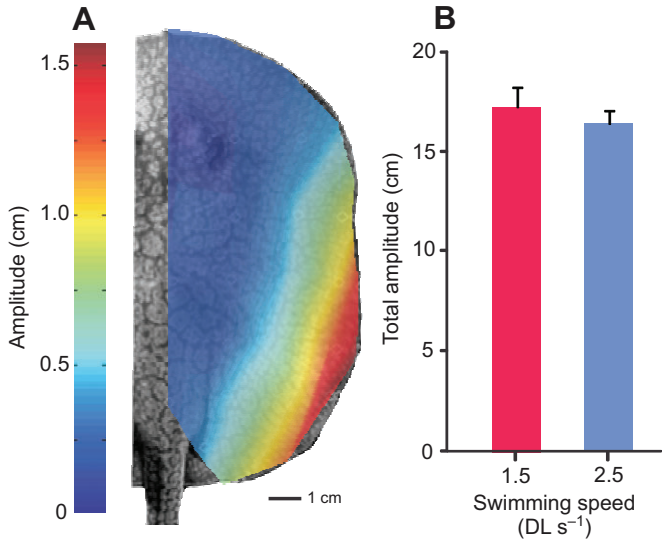

Fig. 5. (A) Amplitude variation across the pectoral fin surface; warmer colors represent greater magnitudes. Amplitude values represent one-half of the maximum excursion occurring at each point during one wave cycle. As no significant differences in amplitude were found between swimming speeds, data were pooled (N=24). (B) Total amplitude, defined as the sum of the amplitudes of all points on the fin, at each speed (N=12, P>0.05); error bars represent 1 s.e.m.

DISCUSSION

Undulatory swimmers propel themselves by passing a wave of bending along a flexible fin or body surface; modulations of the wave produce changes in swimming speed or instigate maneuvers. In undulating rays, the broad, flexible pectoral fins allow for substantial variation in waveform as the propulsive wave propagates across the fin surface. These 3-D deformations cannot be described by a single point or the motion of the fin margin alone. Here we present the first 3-D kinematic analysis of undulatory locomotion in stingrays, determining the properties of the pectoral wave across the entire fin surface and identifying the changes in waveform that drive increased swimming speed (Figs 2–4). In addition, we provide supplementary data sets (supplementary material Tables S1, S2, Fig. S1) describing excursions of the entire pectoral fin surface, which may be useful for future robotic works drawing inspiration from undulating, rajiform swimmers.

Undulations of the pectoral surface

The dramatic undulations of stingray pectoral fins draw attention from any observer – the entire fin initially appears to be involved in a high-amplitude wave (Figs 2, 3). Yet our analysis of 3-D fin surface kinematics reveals that wave amplitude reaches a maximum of 1.66±0.04 cm, or 0.15 DW, and that significant undulations (amplitude >0.5 cm) are restricted to a relatively small portion of the fin, roughly one-quarter to one-third of the total surface, centered on the distal-medial and distal-posterior quadrants of the disc (Fig. 5). Given the size of the fin, a maximum amplitude of less than 2 cm seems small, but still represents a significant fraction of disc width, and is in the range of standardized mid-disc amplitudes found for other batoids (Rosenberger, 2001). Constraints in fin undulation result from a combination of morphological and hydrodynamic factors. First, the central portion of a stingray's body cannot undulate (in dorsoventral or mediolateral directions) due to a stiffened vertebral column and the fusion of the pectoral girdles with axial cartilages (Compagno, 1999); motion of the medial fin is limited by its attachment to the fixed midline. Further, anterior portions of the disc that move freely during other behaviors, such as foraging (Wilga et al., 2012), are held motionless during undulatory locomotion. Minimizing the undulation of the anterior fin during locomotion creates a stable leading edge, streamlining the shape of the body as projected into the water flow, reducing flow separation and drag.

The motion of the pectoral fin increases at mid-disc and posterior regions (Fig. 5). Amplitude increase is nearly linear along the mediolateral axis of the fin, except at the distal margin, where the rate of increase becomes steeper (Fig. 6). This distal increase is an effect of lateral curvature of the fin margin, discussed below. Along the anteroposterior axis, amplitude increases to its maximum value just posterior to mid-disc (at 0.7 DL), and remains near this asymptote from 0.5 to 1.0 DL (Fig. 7). The magnitude of the asymptote varies with position from the midline (due to varying angular displacement), but the pattern holds across the entire disc, in an interesting complement to patterns of amplitude increase found for other undulating swimmers. In eels, amplitude increases continuously along the entire length of the body, without asymptote (Gillis, 1996; Gray, 1933). In the blue-spot stingray, *T. lymma*, amplitude at the fin margin increases towards the mid-disc, and then decreases as the wave moves further posterior; the authors describe this pattern of amplitude increase and decrease as a form of 'narrow-necking' (Rosenberger and Westneat, 1999). Lighthill's original discussion of narrow-necking is in relation to the caudal

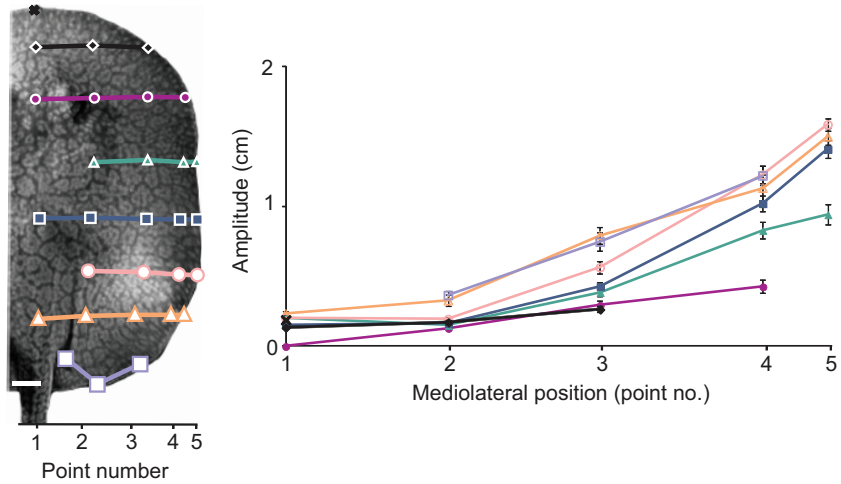

Fig. 6. Spanwise amplitude variation along the mediolateral axis at positions indicated on the stingray image. For clarity, the vertical axis is elongated by a factor of three relative to true aspect ratio. As no significant differences in amplitude were found between swimming speeds, data were pooled (N=24). Error bars represent ±1 s.e.m.; some are obscured by symbols. Scale bar (for the stingray image), 1 cm.

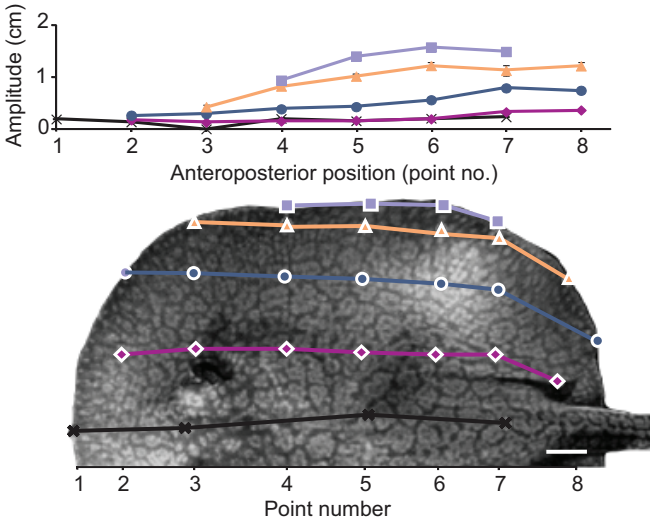

Fig. 7. Chordwise amplitude variation along the anteroposterior axis at positions indicated on the stingray image. As no significant differences in amplitude were found between swimming speeds, data were pooled (*N*=24). Error bars represent ±1 s.e.m.; some are obscured by symbols. Scale bar (for the stingray image), 1 cm.

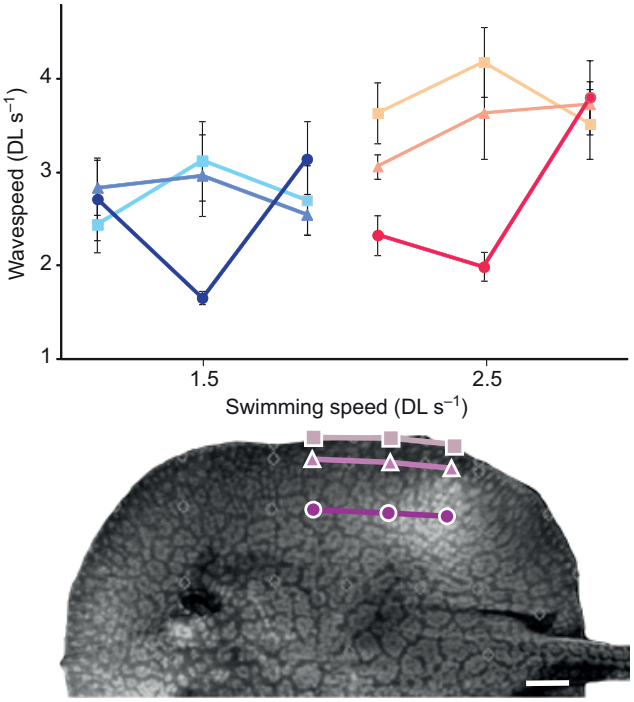

Fig. 8. Wavespeed variation along the anteroposterior axis of the pectoral disc for each swimming speed, at distal (light blue/red), intermediate (medium blue/red) and near-medial (dark blue/red) positions as indicated on the stingray image. Position markers are positioned halfway between the two digitized points used to calculate each local wavespeed. Error bars represent ±1 s.e.m.; *N*=12. Scale bar (for the stingray image), 1 cm.

peduncle of fish swimming *via* body-caudal fin propulsion: a reduction in body depth in regions of high amplitude motion, and/or an increased body depth at the center of mass, reduces recoil forces and yawing moments, reducing drag (Lighthill, 1975). Rosenberger and Westneat suggest that the posterior amplitude decrease seen in *T. lymma* might have a similar effect to reduced body depth, decreasing drag (Rosenberger and Westneat, 1999). However, the broad, dorsoventrally compressed stingray body has ample inertia and added mass to resist recoil forces, and any drag reduction benefit from restricted amplitude is more likely to result from a decrease in projected area, compared with the anguilliform pattern of continuous amplitude increase. The asymptotic amplitude pattern we observe in *P. orbignyi* would reduce projected area, even without the posterior decrease seen in *T. lymma*: as amplitude nears the asymptote, projected area does not increase further. Most importantly, though, the amplitude pattern presented for *T. lymma* highlights the limitations of 2-D analyses when interpreting 3-D waveforms. In Rosenberger and Westneat's study (Rosenberger and Westneat, 1999), measurements were made along the curved fin margin only; the decrease in amplitude between mid-disc (the location of maximum disc width) and the posterior fin may represent nothing more than geometry, because the angular displacement of the fin margin will decrease as the disc narrows. By analyzing points across the fin surface, and comparing points with similar potential for angular displacement, we verify an asymptotic amplitude pattern for *P. orbignyi*: amplitude is constrained, but not reduced, as the propulsive wave crosses the posterior portion of the disc.

Stingrays swim with a mean slip of 0.7±0.04, within the 0.6–0.9 range previously determined for *T. lymma* (Rosenberger and Westneat, 1999), similar to skates (Daniel, 1988) and eels (Gillis, 1996). Our results for wave frequency and mid-disc wavespeed also fall in the range for species studied by Rosenberger (Rosenberger, 2001). We further examined wavespeed in detail, calculating distal, intermediate and medial wavespeeds for the mid-disc region. Within this small region of the fin we found only one significant difference – a posterior increase in medial wavespeed (ANOVA, P=0.0001) – but the overall trend speaks to the path of the propulsive wave across the fin surface (Fig. 8). At both distal and intermediate positions, wavespeeds remain constant across the anteroposterior axis of the examined region. However, at both swimming speeds, medial wavespeeds show the same trend, decreasing from anterior to mid-disc, and then increasing from mid-disc towards the posterior. Though the wavespeed 'trough' does not differ from surrounding values by a statistically significant margin, it does suggest the radial path taken by the propulsive wave, which moves around the perimeter of the disc rather than parallel to the midline. As local wavespeeds were calculated between points on a direct anteroposterior axis, a propulsive wave moving parallel to the midline should have constant wavespeed between all points. A radially propagating wave, however, when measured along a direct anteroposterior axis, would appear to have greater wavespeed when traveling at a greater angle to that axis, i.e. anterior or posterior to the mid-disc region where fin margin and midline are parallel. This is the pattern we observe for medial wavespeeds; we were unable to detect a similar trend for more distal regions of the fin, but the medial pattern corresponds to our direct observations of propulsive wave travel. Frames from a sample sequence, color-coded for velocity, also show heightened wavespeeds along the perimeter of the disc compared with medial regions, further illustrating the radial path of the propulsive wave (Fig. 3).

The importance of considering the direction of wave propagation also emerges in the calculation of wave number, the major metric of batoid locomotion used to describe the oscillatory–undulatory continuum (Rosenberger, 2001). When wave number is calculated relative to disc length (*sensu* Rosenberger, 2001), our data yield a wave number of 1.10±0.08 for *P. orbignyi*, representing just over one complete wave on the

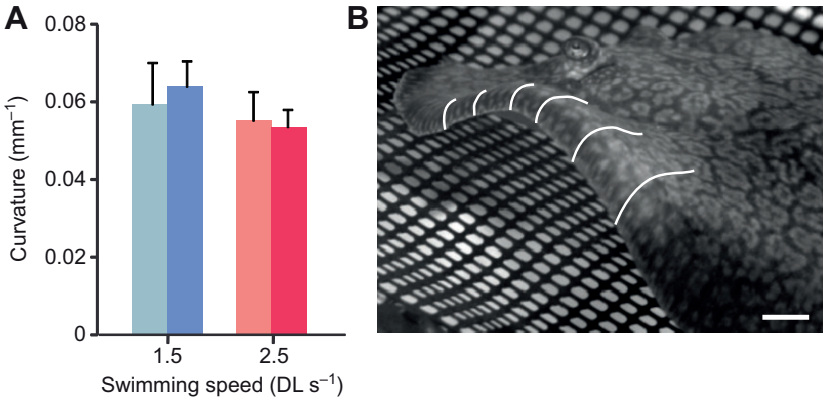

Fig. 9. (A) Magnitude of positive (light blue/red) and negative (deep blue/red) mediolateral fin curvature at both swimming speeds, with no significant differences by curvature sign or speed (P>0.05). Error bars represent 1 s.e.m. (B) Sample frame from high-speed video sequence of stingray swimming. White lines highlight extreme negative curvature at the distal margin of the fin. Scale bar, 1 cm.

pectoral fin at one time, barely above the cut-off of 1 for oscillatory rays. *Potamotrygon orbignyi* is clearly an undulatory swimmer; images of swimming rays reveal significantly more than one wave present on the pectoral fin (Fig. 2). We suggest that rather than calculating wave number relative to disc length, disc perimeter is a more meaningful parameter for *P. orbignyi*, as it better represents the length over which the wave travels. This method yields a wave number of 1.65±0.12, congruent with images of swimming stingrays and firmly within the undulatory region of the continuum. Future studies calculating this value should consider the path of wave travel when selecting a method of standardization.

For a fully detailed description of pectoral surface undulation, we offer an extensive table of pectoral fin excursions beyond the results discussed here (supplementary material Table S1, with point locations given in Fig. S1), as well as a sample data set giving the motion of surface through time (supplementary material Table S2; animation shown in supplementary material Movie 1).

Mediolateral fin curvature

In addition to anteroposterior bending associated with the propulsive wave, notable mediolateral curvature of pectoral fin radials occurs during swimming by *P. orbignyi* (Figs 9, 10). Curvature varies across the mediolateral axis, increasing dramatically near the distal margin. Calculated values (Fig. 9A) underestimate curvature because of the limited resolution available given the number of points digitized on the distal fin, but we observed dramatic distal curvature directly (Fig. 9B) and as changes in the rate of amplitude increase near the distal margin of the fin, where amplitude increases more sharply than in medial regions (Fig. 6).

Changes in cuvature along the length of a fin element, whether the cartilaginous fin radial of an elasmobranch or the bony lepidotrichia of an actinopterygian fish, can result from direct muscle action or inherent structural features. In actinopterygians, the jointed, bilaminar structure of lepidotrichia translates small changes in the length of muscles at the fin base into dramatic fin curvature (Alben et al., 2007; Geerlink and Videler, 1986). This structure-mediated curvature plays a major role in labriform locomotion by the bluegill sunfish, *Lepomis macrochirus*: by curving into a cupped position, the pectoral fins are able to produce net thrust throughout the fin cycle, rather than incurring net drag as the fin abducts (Lauder and Madden, 2007). Skeletal structure also determines flexibility in the pectoral fins of longhorn sculpin, *Myoxocephalus octodecimspinosus*, where variations in segmentation and hemitrich cross-section along the length of individual fin rays allow regionalization of fin function by creating local changes in stiffness (Taft, 2011; Taft et al., 2008). Batoid fin elements lack the bilaminar structure of actinopterygian fin rays and, as seen in *T. lymma*, the muscles that control fin adduction/abduction are not confined to the fin base but extend across the full length of the fin radials (Rosenberger and Westneat, 1999). Therefore, muscles may act directly to create distal curvature. Yet mediolateral variations in the structure of fin elements do occur in batoid pectoral fins (Schaefer and Summers, 2005). Among undulating batoids, stingrays and freshwater stingrays (Dasyatidae and Potamotrygonidae) both have reduced cartilage calcification in the distal fin relative to medial positions, reducing fin stiffness near the margin (Schaefer and Summers, 2005). In addition, fin elements bifurcate near the distal margin, further altering fin stiffness (Schaefer and Summers, 2005). Therefore, spanwise curvature in stingray fins is most likely a

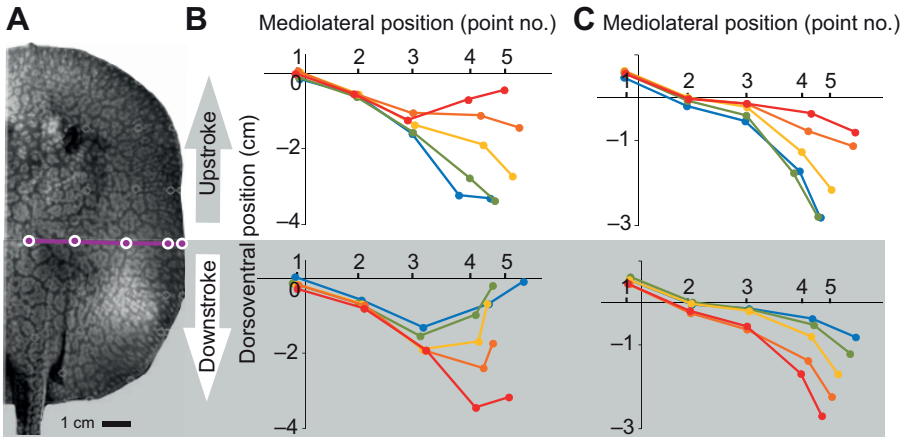

Fig. 10. Sample plots showing fin curvature at the mid-disc mediolateral position indicated on the stingray image (A), as the fin moves dorsoventrally during one wave cycle. Cycles are divided into upstrokes (top row), defined as the portion of the wave cycle where the fin moves from trough to crest, and downstrokes (bottom row), defined from crest to trough. On each plot, colors move from cool to hot (blue to red) through time. Columns illustrate the two major patterns of curvature through one wave cycle: (B) concave down on upstroke, concave up on downstroke, and (C) concave down on upstroke and downstroke.

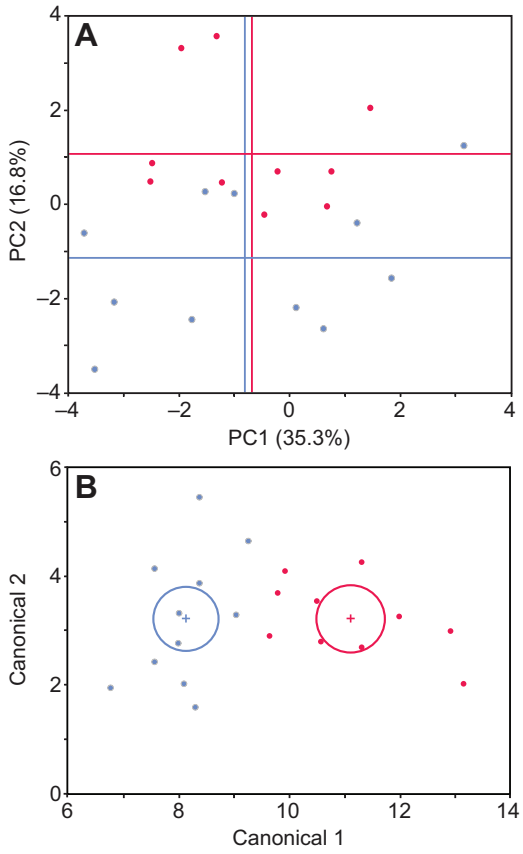

Fig. 11. Multivariate analysis of kinematic variables at swimming speeds of 1.5 DL s^{-1} (blue) and 2.5 DL s^{-1} (red). Each point represents one swimming sequence (N=21). (A) Principal component (PC) plot with significant separation of swimming speeds along PC2 (P<0.001), an axis mainly described by mid-disc wavespeed, mid-disc frequency and the proportion of the cycle spend in negative curvature. Reference lines indicate mean values for each swimming speed on each axis. (B) Discriminant function plot separating swimming speeds along canonical 1 (100% correct classifications), with major influences of mid-disc wavespeed and mid-disc frequency, and secondary influences of mid-disc amplitude, body angle and wavelength. All variables increase from left to right along canonical 1. Ellipses represent 95% confidence intervals with crosshairs at mean values for each speed.

combination of local muscle action and inherent flexibility determined by fin element structure; the exact contributions of each factor are as yet unknown.

In this study we observe two patterns of distal fin curvature during pectoral fin swimming. In the first case, the lateral edge of the fin bends away from the direction of motion, trailing the main portion of the fin. As the fin moves from wave crest to wave trough, the fin margin is curved concave-up; as the fin moves from trough to crest, the margin is curved concave-down (Fig. 10A,B). Therefore, curvature changes direction between upstroke and downstroke. This is the same behavior we would expect from a passive flexible fin, with the edge of the fin bending away from the direction of overall fin motion in response to induced fluid pressure. This pattern of curvature dominates in most swimming sequences, as reflected in the nearly equal portions of the wave cycle spent in positive and negative curvature when all data are combined (59±4% of the cycle in negative curvature). However, in approximately one-third of the sequences the fin retained negative curvature for over 75% of the wave cycle. These sequences exhibit the second pattern of distal curvature we observe in *P. orbignyi*, where concave-down curvature is retained throughout the wave cycle (Fig. 10A,C). Neither this study nor any previous research has collected data on the activity of distal fin musculature during swimming. However, in the second pattern of curvature we observe, fins are curved in opposition to fluid loading. It seems highly likely that this phenomenon is driven by the direct action of local muscles, with passive curvature resulting from inherent fin flexibility determined by fin element structure.

The effects of a similar curvature pattern, with the edges of a flexible fin curved into flow, have been studied using a robotic caudal fin (Esposito et al., 2012). In that study, a motion program in which the dorsal and ventral margins of the caudal fin lead the middle of the fin during swimming results in the caudal fin surface cupping into the flow. Measurements of thrust forces generated during the cupping motion were compared with those produced by the same caudal fin moved as a flat plate. Cupping motions of the fin produced consistently higher thrust forces than the flat plate movement, suggesting that the cupping motion enhances streamwise momentum (Esposito et al., 2012).

In stingrays, retaining a concave-down fin shape is also likely to have hydrodynamic significance, as it will affect flow passing beneath and beside the fin. Compared with a flat fin, distal curvature may improve flow control under the fin by reducing the strength of wingtip vortices, a type of induced drag. Wingtip vortices result from pressure differences between the dorsal and ventral surfaces of an airfoil or hydrofoil; vortices form around the tip of the foil as fluid moves from high to low pressure, circulating around the fin or wing (Vogel, 2003). Though wingtip vortices are most often considered for fixed-wing scenarios, as in aircraft and soaring birds, they also occur at the edge of an undulating fin. In stingrays, the body is held at a positive angle of attack; it acts as a fixed wing, with greater pressure occurring ventrally, and therefore induces wingtip vortex formation. In addition, as most undulating rays typically swim near the substrate, pressure may be increased underneath the fin as it moves from crest to trough and traps fluid between the pectoral disc and the substrate. In aeronautics, various structures are employed to reduce tip vortices or alter their orientation, including the familiar winglets or upswept sections on the wingtips of commercial airliners (Tennekes, 1997). The tightly curled edge of the stingray fin may have a similar effect; changes in spanwise curvature have been found to affect wingtip circulation during bat flight (Hubel et al., 2010). A curved margin may also help control the direction of flow beneath the fin, keeping the bolus of water accelerated by the propulsive wave aligned towards the posterior. As the propulsive wave propagates around the disc radially, not directly from anterior to posterior, the direction of fluid flow is not always aligned to the direction of thrust. By curling the distal region of the fin downward, stingrays may ‘cup’ the fluid moving under the fin, prevent it from spilling around a flat edge, and reorient spanwise flow towards a more optimal axis.

The variability in curvature pattern is interesting. Concave-down curvature was retained throughout the wave cycle in a significant portion of sequences, but not in all; yet if a cupped fin margin offers a hydrodynamic advantage to swimming rays, increasing thrust or reducing drag, we would expect it to be ubiquitous. All individuals were capable of swimming with consistent concave-down curvature, and stingrays were no more or less likely to employ this pattern of curvature as swimming speed increased (ANOVA, P>0.3), contrary to the expectation that increased locomotor demands would elicit it more often. This variability may indicate that the hydrodynamic benefit of swimming with a curled fin is limited.

Variations with swimming speed

In general, fish can increase thrust by varying the frequency or amplitude of the motion of a propulsive surface, or even the area of the surface itself (Bainbridge, 1958; Webb, 1975; Lauder, 2006). For the majority of studied fish species, increases in swimming speed are driven by increases in the frequency of propulsive motions [typically tailbeat frequency (Bainbridge, 1958; Drucker and Jensen, 1996)]. However, the previous study of *T. lymma* found significant individual variability in the wave parameters driving increased swimming speed, with velocity appearing frequency-dependent in some stingrays and amplitude-dependent in others (Rosenberger and Westneat, 1999). In the present study, we find that locomotion by undulatory stingray *P. orbignyi* is decidedly frequency-driven: the mid-disc frequency of the propulsive wave increases by 50% when swimming speed increases by 65%, a highly significant variation (2.53±0.16 to 3.80±0.18 Hz; ANOVA, $P<0.0001$; Fig. 4B). Mid-disc wavespeed increased by the same proportion (31.00±2.53 to 46.02±3.25 cm s^{-1}; ANOVA, $P<0.01$; Fig. 4C). Mean wavelength, the ratio of wavespeed to frequency, therefore remained constant across speeds (12.5±0.7 cm, ANOVA, $P=0.89$). Contrary to some findings for *T. lymma* (Rosenberger and Westneat, 1999), amplitude does not vary between swimming speeds in *P. orbignyi*, whether considered as maximum amplitude, mid-disc amplitude or for any point across the disc (all $P>0.05$; Fig. 4A), excepting one point near the posterior margin, which is unlikely to play a significant role in propulsion, though it may influence flow separation from the fin. One might conjecture that amplitude remains constant because stingrays have maximized potential excursion at the lower swimming speed, and cannot further expand the range of motion. Our data contradict this idea: potential excursion should correspond to angular displacement, increasing with fin span, yet maximum amplitude occurs posterior to the maximum disc width (0.7 *versus* 0.5 DL). We conclude that the amplitude of undulations is not maximized at either swimming speed, and could be increased if changes in swimming velocity were amplitude-driven. The lack of amplitude increase therefore confirms frequency as the driver of increased swimming speed in stingrays, in agreement with the majority of studied fish species (Bainbridge, 1958; Drucker and Jensen, 1996). Increases in the amplitude of propulsive motions, whether a trout's tailbeats or a stingray's undulations, increase projected area and therefore increase drag; a higher swimming speed resulting from increased amplitude would only heighten the drag effect. Frequency-driven increases in velocity do not increase projected area, and are therefore employed by many swimmers as a more efficient means of increasing thrust.

Univariate and multivariate analyses (PCA and DFA) concurred that frequency and wavespeed are the main wave parameters influencing swimming speed (Fig. 11). Mean values of the principal component described by frequency and mid-disc wavespeed differed significantly between swimming speeds (ANOVA, $P<0.01$; Fig. 11A). The DFA correctly identified the swimming speed of 100% of sequences based on frequency and wavespeed data, but was also influenced by mid-disc amplitude and wavelength values despite the lack of significant by-speed differences in the latter two variables when considered independently (ANOVA; Fig. 11B). Given the flexibility of the stingray pectoral disc, it is not surprising that fin modulations may be subtle. The major changes in waveform that determine velocity (frequency and wavespeed) may be accompanied by minor changes in secondary parameters such as amplitude and wavelength.

As stingrays swim faster, the angle between the body and oncoming flow increases slightly but significantly, from 5.18±1.05 to 7.75±0.73 deg (ANOVA, $P<0.05$; Fig. 4D). It is important to note that the magnitude of these values represents the angle between the dorsal surface of the stingray and the oncoming flow, as all digitized points were positioned dorsally. This yields higher body angles than would be calculated from the flat ventral surface, as stingray body depth decreases from head to tail; a sagittal cross-section through the midline would resemble an airfoil, with a flat ventral surface and cambered dorsal surface. However, as the effect of body depth is constant between speeds, the positive correlation between body angle and swimming speed stands. Elasmobranchs are known to use their bodies as lift-generating surfaces; among oscillatory rays (Myliobatidae), pitching of the body can be used to generate thrust (Heine, 1992), and in leopard and bamboo sharks (*Triakis semifasciata* and *Chiloscyllium punctatum*), a positive body angle offsets torques generated by the heterocercal tail (Wilga and Lauder, 2002). In stingrays, a slightly positive body angle will allow their bodies to act as hydrofoils too, generating lift that may counterbalance inherent negative buoyancy or uneven torques produced during locomotion. Yet if the body surface is used to generate a constant amount of lift, we would expect body angle to decrease with speed, not increase, as the amount of lift generated at a given angle of attack increases with flow speed. If the slight change in body angle is robust, stingrays experience increasing lift force as they swim faster, perhaps offsetting a change in torques produced by the pectoral fin.

Our analysis reveals that frequency and wavespeed – the two main drivers of swimming speed in *P. orbignyi* – are accurately represented by mid-disc values, but that major features of pectoral fin undulation can only be described when the fin is considered as a 3-D undulating surface. Several 3-D phenomena have significant implications for the hydrodynamics of rajiform locomotion, including active mediolateral fin curvature and an asymptotic pattern of amplitude variation along the pectoral fin, aspects of waveform that cannot be inferred from a 2-D analysis. We also note that only a relatively small proportion of the fin undulates with significant amplitude. Incorporating these findings into future models of undulating fins will allow further investigation of their hydrodynamic impacts; 3-D studies of other undulators may reveal convergent locomotor strategies for waveform modulation.

LIST OF SYMBOLS AND ABBREVIATIONS

DL	disc length
DP	disc perimeter
DW	disc width
f	frequency
s	three-point curve used to calculate κ
$\mathbf{T}$	unit tangent vector of curve s
U	overall swimming speed
v	wavespeed
κ	curvature
λ	wavelength

ACKNOWLEDGEMENTS

We thank E. M. Standen, J. Lim, N. Danos and B. Flammang-Lockyer for helpful conversations during both the data collection and analysis phases of this work, as well as A. Stubbs for assistance during experiments. We are grateful for the biological illustration work of L. Meszoly, and for valuable advice on stingray species from P. Petry, K. Hartel and A. Williston of the Ichthyology Collection at the Harvard University Museum of Comparative Zoology.

FUNDING

Funding for this project was provided by the National Science Foundation [EFRI-0938043 to G.V.L.], in addition to support from the Harvard University Department of Organismic and Evolutionary Biology, NSF-IGERT Training Grant in Biomechanics and Robert A. Chapman Memorial Scholarship [to E.L.B.].

REFERENCES

Alben, S., Madden, P. G. A. and Lauder, G. V. (2007). The mechanics of active fin-shape control in ray-finned fishes. *J. R. Soc. Interface* **4**, 243-256.

Bainbridge, R. (1958). The speed of swimming of fish as related to size and to the frequency and amplitude of the tail beat. *J. Exp. Biol.* **35**, 109-133.

Breder, C. M. (1926). The locomotion of fishes. *Zoologica* **50**, 159-297.

Clark, R. P. and Smits, A. J. (2006). Thrust production and wake structure of a batoid-inspired oscillating fin. *J. Fluid Mech.* **562**, 415-429.

Compagno, L. J. V. (1999). Endoskeleton. In *Sharks, Skates and Rays: The Biology of Elasmobranch Fishes* (ed. W. C. Hamlett), pp. 69-92. Baltimore, MD: John Hopkins University Press.

Curet, O. M., Patankar, N. A., Lauder, G. V. and MacIver, M. A. (2011). Mechanical properties of a bio-inspired robotic knifefish with an undulatory propulsor. *Bioinspir. Biomim.* **6**, 026004.

Daniel, T. L. (1988). Forward flapping flight from flexible fins. *Can. J. Zool.* **66**, 630-638.

Drucker, E. G. and Jensen, J. (1996). Pectoral fin locomotion in the striped surfperch. I. Kinematic effects of swimming speed and body size. *J. Exp. Biol.* **199**, 2235-2242.

Esposito, C. J., Tangorra, J. L., Flammang, B. E. and Lauder, G. V. (2012). A robotic fish caudal fin: effects of stiffness and motor program on locomotor performance. *J. Exp. Biol.* **215**, 56-67.

Geerlink, P. J. and Videler, J. J. (1986). The relation between structure and bending properties of teleost fin rays. *Neth. J. Zool.* **37**, 59-80.

Gillis, G. B. (1996). Undulatory locomotion in elongate aquatic vertebrates: anguilliform swimming since Sir James Gray. *Am. Zool.* **36**, 656-665.

Gray, J. (1933). Studies in animal locomotion. I. The movement of fish with special reference to the eel. *J. Exp. Biol.* **10**, 88-104.

Harris, J. E. (1936). The role of the fins in the equilibrium of the swimming fish. I. Wind tunnel tests on a model of *Mustelus canis* (Mitchell). *J. Exp. Biol.* **13**, 476-493.

Hedrick, T. L. (2008). Software techniques for two- and three-dimensional kinematic measurements of biological and biomimetic systems. *Bioinspir. Biomim.* **3**, 034001.

Heine, C. E. (1992). Mechanics of flapping fin locomotion in the cownose ray, *Rhinoptera bonasus* (Elasmobranchii: Myliobatidae). PhD thesis, Duke University, Durham, NC, USA.

Hubel, T. Y., Riskin, D. K., Swartz, S. M. and Breuer, K. S. (2010). Wake structure and wing kinematics: the flight of the lesser dog-faced fruit bat, Cynopterus brachyotis. *J. Exp. Biol.* **213**, 3427-3440.

Klausewitz, W. (1965). Die bewegungsweise der geigenrochen – aus funktioneller und stammesgeschichtlicher sicht. *Natur. Mus.* **95**, 97-108.

Lauder, G. V. (2006). Locomotion. In *The Physiology of Fishes*, 3rd edn (ed. D. H. Evans and J. B. Claiborne), pp. 3-46. Boca Raton, FL: CRC Press.

Lauder, G. V. and Madden, P. G. (2007). Fish locomotion: kinematics and hydrodynamics of flexible foil-like fins. *Exp. Fluids* **43**, 641-653.

Lighthill, M. J. (1975). *Mathematical Biofluiddynamics*. Philadelphia, PA: Philadelphia Society for Industrial and Applied Mathematics.

Low, K. H. (2006). Locomotion and depth control of robotic fish with modular undulating fins. *Int. J. Autom. Comput.* **2006**, 348-357.

Macesic, L. J. and Kajiura, S. M. (2010). Comparative punting kinematics and pelvic fin musculature of benthic batoids. *J. Morphol.* **271**, 1219-1228.

Moored, K. W., Dewey, P. A., Leftwich, M. C., Bart-Smith, H. and Smits, A. J. (2011). Bio-inspired propulsion mechanisms based on manta ray locomotion. *Mar. Technol. Soc. J.* **45**, 110-118.

Parson, J., Fish, F. E. and Nicastro, A. J. (2011). Turning performance in batoid rays: limitations of a rigid body. *J. Exp. Mar. Biol. Ecol.* **402**, 12-18.

Roberts, B. L. (1969). The buoyancy and locomotory movements of electric rays. *J. Mar. Biol. Assoc. U. K.* **49**, 621-640.

Rosenberger, L. J. (2001). Pectoral fin locomotion in batoid fishes: undulation versus oscillation. *J. Exp. Biol.* **204**, 379-394.

Rosenberger, L. J. and Westneat, M. W. (1999). Functional morphology of undulatory pectoral fin locomotion in the stingray *Taeniura lymma* (Chondrichthyes: Dasyatidae). *J. Exp. Biol.* **202**, 3523-3539.

Schaefer, J. T. and Summers, A. P. (2005). Batoid wing skeletal structure: novel morphologies, mechanical implications, and phylogenetic patterns. *J. Morphol.* **264**, 298-313.

Standen, E. M. and Lauder, G. V. (2005). Dorsal and anal fin function in bluegill sunfish *Lepomis macrochirus*: three-dimensional kinematics during propulsion and maneuvering. *J. Exp. Biol.* **208**, 2753-2763.

Standen, E. M. and Lauder, G. V. (2007). Hydrodynamic function of dorsal and anal fins in brook trout (*Salvelinus fontinalis*). *J. Exp. Biol.* **210**, 325-339.

Taft, N. K. (2011). Functional implications of variation in pectoral fin ray morphology between fishes with different patterns of pectoral fin use. *J. Morphol.* **272**, 1144-1152.

Taft, N. K., Lauder, G. V. and Madden, P. G. A. (2008). Functional regionalization of the pectoral fin of the benthic longhorn sculpin during station holding and swimming. *J. Zool.* **276**, 159-167.

Taneda, S. and Tomonari, Y. (1974). An experiment on the flow around a waving plate. *J. Phys. Soc. Jpn.* **36**, 1683-1689.

Tennekes, H. (1997). *The Simple Science of Flight.* Cambridge, MA: MIT Press.

Tytell, E. D. and Lauder, G. V. (2004). The hydrodynamics of eel swimming: I. Wake structure. *J. Exp. Biol.* **207**, 1825-1841.

Tytell, E. D., Standen, E. M. and Lauder, G. V. (2008). Escaping Flatland: three-dimensional kinematics and hydrodynamics of median fins in fishes. *J. Exp. Biol.* **211**, 187-195.

Vogel, S. (2003). *Comparative Biomechanics: Life's Physical World*. Princeton, NJ: Princeton University Press.

Webb, P. W. (1975). Hydrodynamics and energetics of fish propulsion. *Bull. Fish Res. Board Can.* **190**, 1-159.

Webb, P. W. (1994). The biology of fish swimming. In *Mechanics and Physiology of Animal Swimming* (ed. L. Maddock, Q. Bone and J. M. V. Rayner), pp. 45-62. Cambridge: Cambridge University Press.

Webb, P. W. (2006). Stability and maneuverability. In *Fish Biomechanics* (ed. R. E. Shadwick and G. V. Lauder), pp. 281-332. Amsterdam: Elsevier.

Wilga, C. D. and Lauder, G. V. (2002). Function of the heterocercal tail in sharks: quantitative wake dynamics during steady horizontal swimming and vertical maneuvering. *J. Exp. Biol.* **205**, 2365-2374.

Wilga, C. D., Maia, A., Nauwelaerts, S. and Lauder, G. V. (2012). Prey handling using whole-body fluid dynamics in batoids. *Zoology* **115**, 47-57.

Wu, C., Wang, L. and Wu, J. (2007). Suppression of the von Kármán vortex street behind a circular cylinder by a travelling wave generated by a flexible surface. *J. Fluid Mech.* **574**, 365-391.